Contribution from the Istituto di Chimica e Tecnologia dei Radioelementi del CNR, Padova, Italy, Department of Chemistry, Northwestern University, Evanston, Illinois, Dipartimento di Chimica Inorganica, Metallorganica ed Analitica, Università di Padova, Padova, Italy, and Istituto di Chimica Generale ed Inorganica, Università di Torino, Torino, Italy

Combined UV-PES and Theoretical Study of Binuclear $M_2(CO)_6(C_4H_4)$ Complexes (M = Fe, Ru, Os)

M. Casarin,*[1a] D. Ajò,[1a] A. Vittadini,[1a] D. E. Ellis,*[1b] G. Granozzi,*[1c] R. Bertoncello,[1c] and D. Osella[1d]

Received July 11, 1986

The gas-phase UV-photoelectron (PE) spectra of binuclear metallacyclopentadienyl derivatives of Fe, Ru, and Os are reported. The assignment of experimental data has been carried out by means of theoretical results with nonrelativistic first-principle DV–Xα calculations. Differences along the investigated series in the metal–metal and metal–ligand interactions allow us to obtain a theoretical explanation of the different structure of the osmium derivative with respect to those of the iron and ruthenium complexes. Moreover, theoretical results point out that the metal–metal bond plays a leading role, influencing not only the strength but also the nature of the metal–ligand interactions. Plots of some molecular orbitals are reported and discussed.

Introduction

The description of the electronic structure of molecular systems containing a pentaatomic metallacycle moiety has received remarkable attention.[2-4] In a systematic investigation of delocalization in metallacycles, Thorn and Hoffmann[3a] have determined requirements for such molecules to show delocalized bonding. In particular, they excluded the presence of significant delocalization in mononuclear metallacyclopentadienyl derivatives on the basis of the estimated inaccessibility of the C_4H_4-localized π_3* molecular orbital (the LUMO of the organic fragment), too high in energy to strongly interact with the HOMO of the inorganic portion. In contrast they indicate binuclear metallacyclopentadienyl complexes (where the second metal atom is π-bound to the metallacycle) as good candidates to show a six-π-electron aromatic ring.

In this paper we report the results of an investigation on the electronic structure of metallacyclopentadienyl binuclear complexes along the series $Fe_2(\mu\text{-}CO)(CO)_5(C_4H_4)$ (**I**, already investigated in a previous paper[4]), $Ru_2(\mu\text{-}CO)(CO)_5(C_4H_4)$ (**II**), and $Os_2(CO)_6(C_4H_4)$ (**III**) by means of gas-phase He I/He II UV-PE spectroscopy and nonrelativistic first-principle DV–Xα calculations. The main aim of this study is the analysis of the bonding scheme inside the metallacycle fragments and the variations of the whole electronic structure along the series. In this regard one has to recall that compounds **I** and **II** have the same structure in the solid state[5a-e,g-h] with the presence of a semibridging carbonyl group, while **III** has a sawhorse geometry[5i,j] with no semibridging carbonyl (see Figure 1).

Experimental Section

Spectra. He I and He II excited PE spectra were measured on a Perkin-Elmer PS-18 spectrometer modified for He II measurements by inclusion of a hollow-cathode discharge lamp giving high output of He II photons (Helectros Developments). The ionization energy (IE) scale was calibrated by reference to peaks due to admitted inert gases (Xe–Ar) and to the He $1s^{-1}$ self-ionization. A heated inlet probe system was adopted at 40–70 °C.

Synthesis. Binuclear derivatives **I**, **II**, and **III** were synthesized according to the published procedures.[6] After crystallization, their purity was checked by IR, ^{1}H NMR, and MS spectroscopy. IR, ^{1}H NMR, and MS spectra were recorded on Perkin-Elmer 580B, JEOL GX 270/89, and EAI MS12 instruments, respectively.

Theoretical Method. Hartree–Fock–Slater (HFS) discrete variational (DV–Xα) calculations[7] on **I**, **II**, and **III** were performed on a VAX-11/750 (Digital Equipment Corp.) computer at the computing center of the Institute of Chemistry and Technology of Radioelements of the CNR.

The approximations of the reported theoretical calculations are (i) use of near-minimal atomic orbital (AO) basis sets, (ii) SCC approximation of Coulomb potential, representing atoms by overlapping spherical charge distributions,[7b] (iii) use of the Gaspar–Kohn–Sham exchange potential,[8] (iv) neglect of correlation terms, (v) neglect of relativistic effects, and (vi) Slater's transition-state (TS) formalism[9] to calculate the IEs.

It is known from extensive studies on organic and metal compounds that improved bases and potential representations lead to improved IEs, molecular binding energy curves, etc.[10] However, primary corrections only produce a uniform level shift.[10] In the present case we found systematic differences between theoretical and experimental IEs, so that we suppose that primary bonding features are adequately determined at the present level of precision.

Numerical AOs (through 4p on Fe, 5p on Ru, 6p on Os, 2p on C and O, and 1s on H) obtained for the neutral atoms were used as basis functions. Due to the size of the investigated systems, orbitals 1s–3p (Fe), 1s–4p (Ru), 1s–5p (Os), and 1s (C and O) were treated as a part of a frozen core in the molecular calculations. Atomic orbital and bond overlap populations (OPs) were computed by using the Mulliken scheme,[11] and they are reported in Table I. Experimental geometries[5] of **I–III** were idealized to C_s symmetry for use in the calculations. The MOs have been labeled then according to the irreducible representations a′ and a″.

Results and Discussion

The electronic structure of complex molecular systems is usually best pursued by making reference to simpler related compounds or fragments. However, the choice of reference fragments may

(1) (a) CNR. (b) Northwestern University. (c) Università di Padova. (d) Università di Torino.
(2) Van Koten, G.; Vrieze, K. *Adv. Organomet. Chem.* **1982**, *21*, 151 and references therein.
(3) (a) Thorn, D. L.; Hoffmann, R. *Nouv. J. Chim.* **1979**, *3*, 39. (b) Trogler, W. C.; Curtis, E. J.; Ellis, D. E. *Inorg. Chem.* **1981**, *20*, 980 and references therein. (c) Gross, M. E.; Trogler, W. C.; Ibers, J. A. *J. Am. Chem. Soc.* **1981**, *103*, 192.
(4) Casarin, M.; Ajò, D.; Granozzi, G.; Tondello, E.; Aime, S. *Inorg. Chem.* **1985**, *24*, 1241.
(5) (a) Hock, A. A.; Mills, O. S. *Acta Crystallogr.* **1961**, *14*, 139. (b) Todd, L. J.; Hickey, J. P.; Wilkinson, J. R.; Huffman, J. C.; Folting, K. *J. Organomet. Chem.* **1976**, *112*, 167. (c) Degrève, Y.; Meunier-Piret, J.; Van Meerssche, M.; Piret, P. *Acta Crystallogr.* **1967**, *23*, 119. (d) Epstein, E. F.; Dahl, L. F. *J. Am. Chem. Soc.* **1970**, *92*, 493. (e) Prince, S. R. *Cryst. Struct. Commun.* **1976**, *5*, 451. (f) Jeffreys, J. A. D.; Willis, C. M. *J. Chem. Soc., Dalton Trans.* **1972**, 2169. (g) Astier, A.; Daran, J. C.; Jeannin, Y.; Rigault, C. *J. Organomet. Chem.* **1983**, *241*, 53. (h) Noda, I.; Yasuda, H.; Nakamura, A. *J. Organomet. Chem.* **1983**, *250*, 447. (i) Harris, P. J.; Howard, J. A. K.; Knox, S. A. R.; Phillips, R. P.; Stone, F. G. A.; Woodward, P. *J. Chem. Soc., Dalton Trans.* **1976**, 377. (j) Dodge, R. P.; Mills, O. S.; Schomaker, V. *Proc. Chem. Soc., London* **1963**, 380.
(6) Aime, S.; Occhiello, E. *J. Chem. Soc., Dalton Trans.* **1986**, 1863.
(7) (a) Averill, F. W.; Ellis, D. E. *J. Chem. Phys.* **1973**, *59*, 6411. (b) Rosen, A.; Ellis, D. E.; Adachi, H.; Averill, F. W. *J. Chem. Phys.* **1976**, *65*, 3629 and references therein. (c) Trogler, W. C.; Ellis, D. E.; Berkowitz, J. *J. Am. Chem. Soc.* **1979**, *101*, 5896.
(8) (a) Gaspar, R. *Acta Physiol. Acad. Sci. Hung.* **1954**, *3*, 263. (b) Kohn, W.; Sham, L. J. *Phys. Rev.* **1965**, *140*, A1133.
(9) Slater, J. C. *Quantum Theory of Molecules and Solids. The Self-Consistent Field for Molecules and Solids*; McGraw-Hill: New York, 1974; Vol. 4.
(10) (a) Delley, B.; Ellis, D. E. *J. Chem. Phys.* **1982**, *76*, 1949 and references therein. (b) Ruscic, B.; Goodman, G. L.; Berkowitz, J. *J. Chem. Phys.* **1983**, *78*, 5443 and references therein.
(11) Mulliken, R. S. *J. Chem. Phys.* **1955**, *23*, 1833.

0020-1669/87/1326-2041$01.50/0

Table I

Comparison of Overlap Populations of I–IV

	M–M′		M–C_1		M–C_3		M–C_5		M–C_6		M′–C_1		M′–C_2		M′–C_3		M′–C_4		C_3–C_4	
	a′	a″	a′	a″	a′	a″	a′	a″	a′	a″	a′	a″	a′	a″	a′	a″	a′	a″	a′	a″
$Fe(CO)_3(C_4H_6)$											0.48	0.14	0.13	0.18	0.03	0.08	0.00	0.03	0.38	0.52
$Fe_2(CO)_6(C_4H_4)$	0.06	−0.03	0.15	−0.01	0.28	0.21	0.19	0.23	0.29	0.08	0.11	0.12	0.13	0.15	0.10	0.09	−0.17	0.03	0.35	0.52
$Ru_2(CO)_6(C_4H_4)$	0.12	−0.02	0.14	0.00	0.32	0.24	0.21	0.21	0.21	0.10	0.31	0.10	0.21	0.24	0.06	0.10	−0.07	0.03	0.41	0.53
$Os_2(CO)_6(C_4H_4)$	0.37	−0.01			0.27	0.24	0.24	0.24	0.30	0.11	0.36	0.14	0.24	0.29	0.07	0.10	−0.01	0.03	0.40	0.55

Comparison of Gross Atomic Charges of I–IV

	M	M′	C_1	C_2	C_3	C_4	C_5	C_6	O_1	O_2	O_5	O_6
$Fe(CO)_3(C_4H_6)$		1.083	−0.132	−0.057	−0.616	−0.282			−0.171	−0.132		
$Fe_2(CO)_6(C_4H_4)$	1.095	1.063	−0.185	−0.030	−0.647	−0.286	−0.049	0.038	−0.167	−0.184	−0.176	−0.165
$Ru_2(CO)_6(C_4H_4)$	0.632	0.700	−0.008	0.075	−0.514	−0.256	0.073	0.146	−0.201	−0.205	−0.211	−0.200
$Os_2(CO)_6(C_4H_4)$	0.823	0.840	−0.015	0.011	−0.566	−0.223	−0.021	0.104	−0.184	−0.189	−0.203	−0.202

Table II. Atomic Character from the SCC DV-Xα Calculation for $Fe(CO)_3(C_4H_6)$

			population, %							
			Fe							
MO	eigenvalue, $-E$, eV	TSIE, eV	s	p	d	2 C_3	2 C_4	6 H	3 CO	character
18a′	5.75	9.47	0	10	41	30	4	4	11	Fe → π_3*
17a′	6.56	10.24	0	7	58	3	1	2	29	3d t_{2g}-like MOs
12a″	6.66	10.35	0	4	58	10	0	2	26	
16a′	6.76	10.67	1	3	60	5	8	0	22	
11a″	7.64	11.59	0	1	18	50	24	1	6	π_2
15a′	9.16	12.94	0	1	3	11	68	2	15	π_1

Table III. Atomic Character from the SCC DV-Xα Calculation for $Fe_2(CO)_6(C_4H_4)$

			population, %											
			Fe			Fe′								
MO	eigenvalue, $-E$, eV	TSIE, eV	s	p	d	s	p	d	2 C_3	2 C_4	4 H	$(CO)_1$	5 CO	character
29a′	6.48	9.05	1	11	35	0	1	16	8	0	0	8	20	Fe + Fe′ + π_3*
19a″	6.59	9.08	0	0	43	0	4	18	12	4	0	4	15	
28a′	7.04	9.54	0	0	67	0	0	6	1	2	2	0	22	
27a′	7.23	9.84	0	0	5	0	8	55	1	2	1	11	17	3d t_{2g}-like MOs
26a′	7.45	10.16	0	0	4	0	7	59	3	3	1	1	22	
18a″	7.67	10.24	0	0	19	0	2	44	4	3	0	14	14	
25a′	7.91	10.49	0	2	41	0	1	11	14	6	2	5	18	
17a″	8.46	10.94	0	3	14	0	0	12	41	14	1	0	15	π_2
16a″	9.44	11.94	0	3	10	0	3	3	51	6	6	6	12	n−
24a′	9.82	12.32	0	2	3	0	3	3	36	27	3	7	16	n+
23a′	10.16	12.59	0	2	2	0	1	8	18	34	2	11	22	π_1

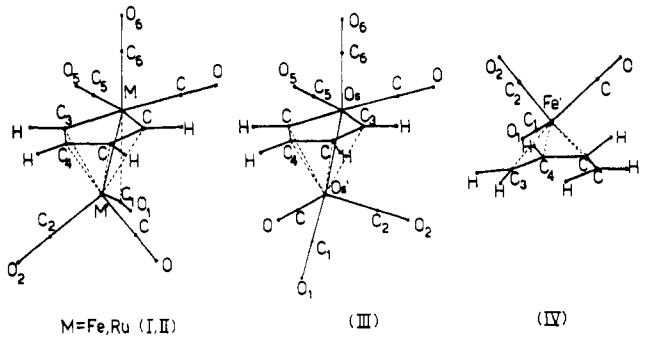

Figure 1. Numbering scheme used for **I–IV**.

tend to emphasize a particular interaction rather than another one. Actually, this is what occurred in previous studies of **I**, where the attention was focused either on the perturbations in the $M_2(CO)_6$ fragment energy levels due to the C_4H_4 ligand[12] or on the interactions between the fragments $Fe(CO)_3$ and $Fe'(CO)_3(C_4H_4)$.[4] The latter choice took advantage of the strong similarity between the $Fe'(CO)_3(C_4H_4)$ fragment and tricarbonyl(butadiene)iron (hereafter indicated by **IV**), a molecule whose electronic structure was extensively investigated in the past both experimentally and theoretically.[13]

Believing that a satisfactory understanding of the electronic structure of the title molecules would come through a comparison with the bonding scheme of **IV**, we decided to perform a further investigation of its electronic structure[14] in order to compare homogeneous theoretical results.

The charge density analysis of the six outermost MOs of **IV** is reported in Table II.[16] The 18a′ HOMO, mainly localized on the iron and terminal carbon atoms of the organic ligand, accounts for the Fe′ → π_3* back-bonding interaction. The three subsequent MOs (17a′, 12a″, 16a′) are strongly localized on the metal atom (d pairs), while 11a″ and 15a′ eigenvectors are related to the free ligand π_2 and π_1 MOs,[17] respectively. The iron participation in the 15a′ MO is very small, pointing out that the π → Fe′ donation involves substantially only the ligand-based π_2 MO and that the suggested repulsion between π_1 and the suitable d pair[12a,13a] is negligible (Table II). Reference to gross atomic charges reported in Table I shows that, in agreement with the well-known elec-

(12) (a) Elian, M.; Hoffmann, R. *Inorg. Chem.* **1975**, *14*, 1058. (b) Thorn, D. L.; Hoffmann, R. *Inorg. Chem.* **1978**, *17*, 126.

(13) (a) Connor, J. A.; Derrick, L. M. R.; Hall, M. B.; Hillier, I. H.; Guest, M. F.; Higginson, B. R.; Lloyd, D. R. *Mol. Phys.* **1974**, *28*, 1193. (b) Boehm, M. C. *J. Phys. B* **1984**, *17*, 3103. (c) Boehm, M. C. *J. Chem. Phys.* **1983**, *78*, 7044. (d) Boehm, M. C. *THEOCHEM* **1983**, *9*, 73.

(14) The experimental geometry[15] was idealized to C_s symmetry for use in the calculations.

(15) Mills, O. S.; Robinson, G. *Acta. Crystallogr.* **1963**, *16*, 758.

(16) In spite of the low molecular symmetry, the a′ and a″ MO labeling allows us to distinguish the π_3* and/or π_1 (both a′ in symmetry) involvement from that of π_2 (a″) in the metal–ligand interaction.

(17) Turner, D. W.; Baker, A. D.; Brundle, C. R. *Molecular Photoelectron Spectroscopy*; Wiley: New York, 1970.

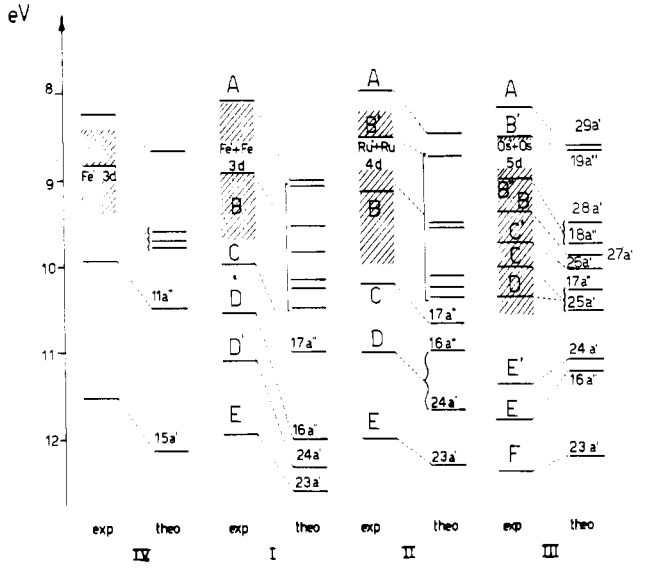

Figure 2. Comparison between experimental and computed transition-state ionization energies for **I–IV**.

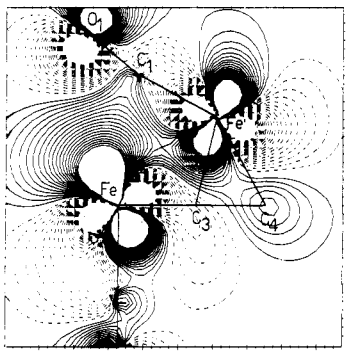

Figure 3. Contour plot for the 29a′ MO in the *XZ* plane. The interval between successive contour levels is 0.0337 $e^{1/2}/Å^{3/2}$.

tron-donating properties of the Fe′$(CO)_3$ fragment,[12] the butadiene ligand is negatively charged.

In relation to He I/He II PE results published by Connor et al.,[13a] the assignment they proposed agrees quite well with our transition-state ionization energy (TSIE) calculations (Figure 2). The unique discrepancy is related to the assignment of the shoulder (8.23 eV) lying on the lower IE side of the first band. Actually, we find the HOMO significantly localized on the organic moiety while the shoulder had been assigned to the ionization from a metal d pair. In this regard, it is noteworthy that literature all-electron ab initio calculations (ground-state and ΔSCF calculations)[13a] indicate for the HOMO a substantial butadiene character.

$Fe_2(\mu$-CO)$(CO)_5(C_4H_4)$. Encouraged by the agreement between TSIE results and experimental PE data relative to **IV**, and by the possibility of comparing theoretical results along the series **I–III**, we decided to perform a DV–Xα theoretical investigation of **I**, to supplement the Hartree–Fock (HF) study of its electronic structure recently published by some of us.[4] The charge density analysis of the 11 outermost MOs of **I** is reported in Table III, where the same MO identifications used in the previous investigation[4] have been adopted. Moreover, because of the high complexity of the covalent pattern due to low symmetry of the molecule, in the forthcoming theoretical analysis we will make use of MO contour plots (CPs), which are very useful in order to assess the nature of the selected MOs.

In Figure 3 we report the CP of the 29a′ HOMO in the symmetry plane containing the iron atoms and the semibridging carbonyl group. The analysis of the figure shows the high delocalization of this MO, which represents at the same time metals → π_3*, metals → $\pi^*(C_1–O_1)$ back-bonding, and Fe–Fe′ interactions. Such a picture of the HOMO is in agreement with the well-known π-acceptor capability of semibridging carbonyls.[18]

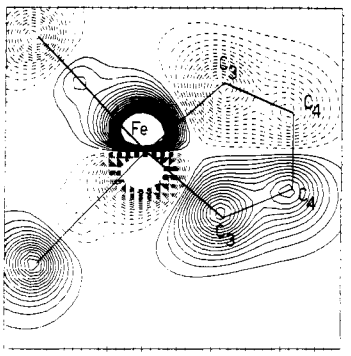

Figure 4. Contour plot for the 19a″ MO in the *XY* plane. The plot represents a slice 1 au above the FeC_4H_4 ring. Plot parameters are identical with those of Figure 3.

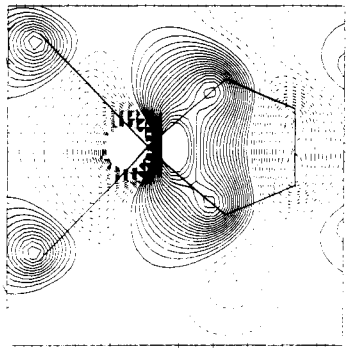

Figure 5. Contour plot for the 25a′ MO in the *XY* plane. The plot represents a slice 1 au above the FeC_4H_4 ring. Plot parameters are identical with those of Figure 3.

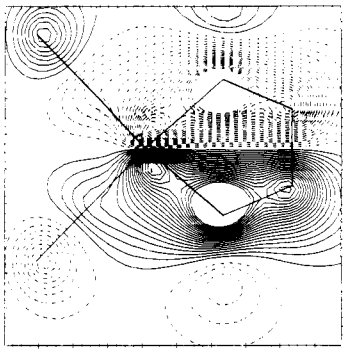

Figure 6. Contour plot for the 17a″ MO in the *XY* plane. The plot represents a slice 1 au above the FeC_4H_4 ring. Plot parameters are identical with those of Figure 3.

Going on with the eigenvector analysis, we note a very interesting behavior showed by the six atomlike MOs (d pairs) 19a″–25a′ (Table III) in relation to their spatial and energy localization. In fact, the 27a′, 26a′, and 18a″ MOs are very close in energy and all of them are mainly localized on Fe′. In contrast, the 19a″, 28a′, and 25a′ MOs (localized on the cyclic Fe atom) have significantly different energies. Actually the 19a″ and 25a′ MOs are strongly destabilized and stabilized, respectively, with respect to the 28a′ MO, which shows, on its own, the lowest localization percentage in the ligand. Inspection of Figures 4 and 5, where the CPs of the 19a″ and 25a′ MOs 1 au above the metallacycle plane[19] are reported, shows that the former MO is destabilized because of the antibonding interaction (π in character) between the ligand-based π_2 MO and one d pair (Fe d_{yz} in our framework). Incidentally, the bonding counterpart, mainly localized on the organic fragment, is accounted for by the 17a″ MO, whose CP is reported in Figure 6. In contrast, the 25a′ MO

(18) (a) Cotton, F. A. *Prog. Inorg. Chem.* **1976**, *21*, 1. (b) Morris-Sherwood, B. J.; Powell, C. B.; Hall, M. B. *J. Am. Chem. Soc.* **1984**, *106*, 5079.
(19) 1 au is ca. the maximum in the radial distribution function for a 2p orbital.

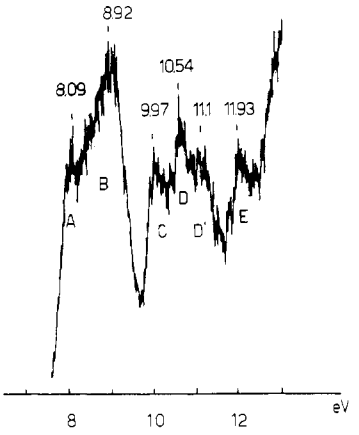

Figure 7. He I PE spectrum of $Fe_2(\mu\text{-}CO)(CO)_5(C_4H_4)$.

is strongly stabilized with respect to the 28a′ one because it represents the Fe d_{xz} pair, which back-donates into the ligand-based π_3* MO. This charge-release mechanism, concomitant with that involving the semibridging carbonyl group (see the HOMO), is not surprising because, on the basis of the EAN (effective atomic number) rule, the Fe atom is formally in the −1 oxidation state.

It is interesting to note that the 25a′ MO can be related to one of the components of the e_1'' π MO of the free cyclopentadienyl (Cp) anion in D_{5h} symmetry. The second component of the e_1'' energy level is associated with the 17a″ MO (see Figure 6), where the Fe atom participates by using dδ AOs. Thence, it is possible to picture the bonding scheme of the ferracycle to be very similar to that of a free Cp anion perturbed by the presence of a heteroatom fitted up with d AOs. The three π-like molecular orbitals responsible for the six-π-electron metalla aromatic ring are then the 25a′, 17a″, and 23a′ ones. This description is correct from an isolobal point of view because, assuming the existence of a dative Fe′→Fe bond,[18] we deal with a $M(CO)_3$ (M is now a d^9 metal) fragment isolobal with a CH fragment.[20] Furthermore, in agreement with Thorn and Hoffmann's anticipation[3a] about the consequences of such delocalization on C–C distances, the three C–C bond lengths of the ligand chain[5a] are virtually identical (3σ for C–C = 0.03 Å). The Fe–C_3 bond distance (1.95 Å) would be consistent with a single bond if the predicted sum of covalent radii, with a trigonally hybridized C atom, (1.24 + 0.74 = 1.98 Å) is assumed. However, such a consideration has scarce significance because the C_3 covalent radii could be influenced by the presence of the Fe′ atom.

Turning our attention now to the analysis of the Fe′–C_4H_4 interaction, we observe that it is stronger in **I** than in **IV** (see OPs in Table I). Actually, even though Fe′–C_3 and Fe′–C_4 bond distances are almost the same in the two complexes (maximum difference ca. 0.1 Å),[5a,15] the total Fe′–C_3 OP passes from 0.19 e (**I**) to 0.11 e (**IV**) with a concomitant increase of the total C_3–C_4 OP (Table I). Dividing the Fe′–C_3 OP into its a′ and a″ contributions,[16] we observe (Table I) that the a″ values are 0.09 and 0.08 e in **I** and **IV**, respectively, while the a′ values are 0.10 and 0.03 e. The similarity of the a″ OP values indicates that the metal–ligand interactions involving the ligand-based π_2 MO are very similar in the two complexes. The increase in the a′ OP value should be ascribed to a higher mixing of Fe′ AOs with the ligand-based π_1 MO (Table III) in **I** compared to **IV**, rather than to a higher Fe′ → π_3* back-donation.[21]

The low-IE region (8–13 eV) of the PE spectrum of **I** is reported in Figure 7. The region above 13 eV (not reported here) consists of a very ill-resolved structure primarily due to ionization from iron–CO σ-bonding MOs and 1π and 4σ CO-localized levels. The analysis of this region is unproductive and is out of the scope of this paper. The assignment proposed in the previous HF investigation[4] is confirmed by means of the present HFS transition-state

(20) Hoffmann, R. *Angew. Chem.* **1982**, *21*, 711.
(21) In **I**, Fe′ is formally involved in the Fe′ → Fe dative interaction and according to the EAN rule it is in the +1 oxidation state.

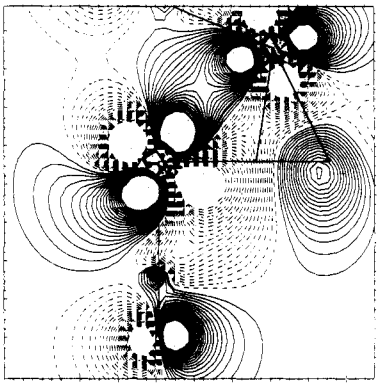

Figure 8. Contour plot for the 25a′ MO in the *XZ* plane of $Ru_2(\mu\text{-}CO)(CO)_5(C_4H_4)$. Plot parameters are identical with those of Figure 3.

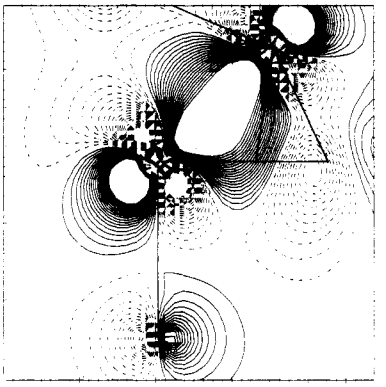

Figure 9. Contour plot for the 24a′ MO in the *XZ* plane of $Ru_2(\mu\text{-}CO)(CO)_5(C_4H_4)$. Plot parameters are identical with those of Figure 3.

calculations. Theoretical IEs are uniformly overestimated here by some 1.0–1.5 eV, but they reproduce quite accurately orbital energy differences (Figure 2). The comparison of the experimental results relative to **I** and **IV** gives support to the aforementioned theoretical considerations about the π_1 mixing in the Fe′–C_4H_4 interaction. Actually, the IE values of the band related to the ionization from the ligand-based π_2 MO are almost exactly the same in **I** and **IV** (9.97 (**I**), 9.93 eV (**IV**)[7a]) while the IE of the ligand-based π_1 MO passes from 11.52 (**IV**)[7a] to 11.93 eV (**I**).

$Ru_2(\mu\text{-}CO)(CO)_5(C_4H_4)$. The comparison between theoretical results of **I** and **II** shows significant differences, mainly related to the M–M′ bond, of the role played by the semibridging carbonyl group and of the metal–ligand interactions present inside the metallacycle. Moreover, because of a stronger mixing between metal and ligand AOs as a consequence of higher covalency, it is impossible in **II** to maintain the same MO labeling adopted for **I**.

Starting with the analysis of the M–M′ interaction, we note (Table I) the significant increase of the M–M′ OP on passing from **I** to **II**. This strengthening of the M–M′ bond must be traced back to the contribution from the inner 25a′ and 24a′ MOs (CPs are reported in Figures 8 and 9, respectively). It is important to notice the different natures of the 24a′ MO in **I** and **II**: in **I** it mainly represents the n^+ combination of the C_3 radical lobes pointing toward the Fe atom, while in **II** it gives origin to a concerted bonding interaction between the two Ru and C_3 atoms (see Figure 9).

As far as the semibridging carbonyl is concerned, reference to the gross atomic charges and OPs reported in Table I shows that the charge-release mechanism involving M and the semibridging carbonyl found in **I** still holds in **II**, but it probably plays a less important role. Such a behavior is expected on the basis of the metallic electronegativity differences (Pauling values: Fe, 1.8; Ru, 2.2)[22] coupled with the possibility of balancing Ru and Ru′

(22) Johnson, B. F. G.; Lewis, J. *Adv. Inorg. Chem. Radiochem.* **1981**, *24*, 225.

Table IV. Atomic Character from the SCC DV-Xα Calculation for $Ru_2(CO)_6(C_4H_4)$

MO	eigenvalue, $-E$, eV	TSIE, eV	population, % Ru s	Ru p	Ru d	Ru′ s	Ru′ p	Ru′ d	2 C_3	2 C_4	4 H	$(CO)_1$	5 CO
29a′	6.11	8.48	0	11	24	0	5	18	11	2	0	7	22
19a″	6.36	8.75	0	0	29	0	3	15	25	10	0	3	15
28a′	7.13	9.52	1	2	62	0	0	6	3	3	2	1	20
27a′	7.18	9.57	0	0	27	0	3	31	1	11	1	7	19
26a′	7.58	10.13	0	0	1	0	3	58	12	0	1	3	22
18a″	7.85	10.26	0	1	35	0	0	22	15	1	1	5	20
25a′	7.96	10.38	0	2	29	0	0	18	23	4	4	5	15
17a″	8.20	10.68	0	2	6	0	0	38	23	8	2	6	15
16a″	8.59	10.99	0	1	21	0	2	5	42	7	3	1	18
24a′	9.26	11.67	1	1	22	0	2	20	31	3	3	3	14
23a′	9.76	12.32	0	0	2	0	0	8	14	64	0	5	7

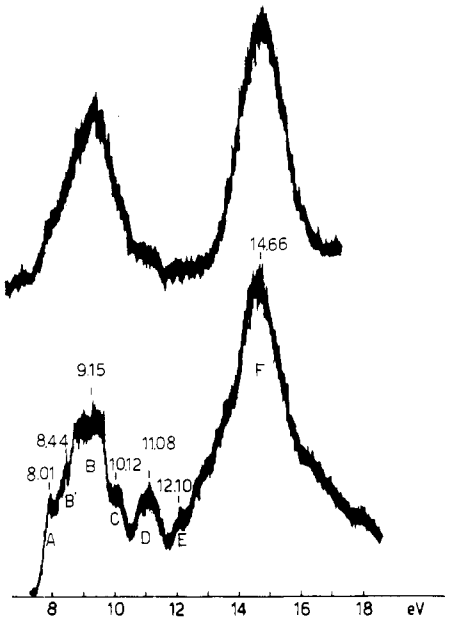

Figure 10. He I (bottom) and He II (top) PE spectra of $Ru_2(\mu\text{-CO})(CO)_5(C_4H_4)$.

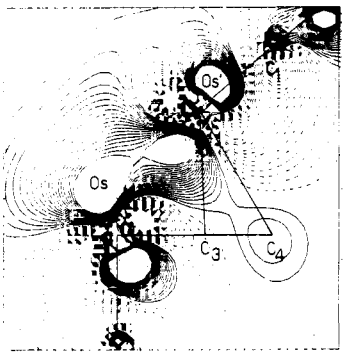

Figure 11. Contour plot of the 29a′ MO in the XZ plane of $Os_2(CO)_6(C_4H_4)$. Plot parameters are identical with those of Figure 3.

charges through direct metal–metal interaction.

Turning now to the ruthenacycle, we note that the aforementioned strong mixing between metal AOs and ligand-based MOs causes a significant rehybridization of C_3 and C_4 atoms that no longer allows any discrimination between σ and π contributions within the cycle and prevents the possibility of picking out three well-defined MOs (mainly π in character) responsible for a six-π-electron metalla aromatic ring as in **I**. Nevertheless, a high degree of charge delocalization has to be present in the butadiene chain of **II** because of the nearly equal (within the experimental deviations) C–C distances found in the solid-state structural determinations.[5g,h] This evidence suggests that two different charge redistribution mechanisms (namely, π delocalization and metal-induced σ/π rehybridization) are both effective in obtaining a bond length equalization within the butadiene chain. Differences in electronegativity and AO spatial extensions of metal atoms control the actual charge redistribution mechanism.

The He I/He II experimental PE data of **II** are reported in Figure 10. The experimental patterns of **I** and **II** are quite different; in the lower IE region of **II** an extra band B′ is now present and band B partially overlaps with band C. Finally, bands D and E in the He I spectrum of **I** give origin to a single band (band D) in **II**. No doubt at all exists in relating bands C, D, and E to ionizations from ligand-based MOs on the basis of their dramatic decrease in relative intensity on passing from the He I to the He II ionization source.[23] Making reference to the assignments of **I** and to the TSIEs[25] of **II** (Table IV and Figure 2), we propose to assign bands C and E each to a single ionization event (17a″ and 23a′ MOs, respectively) while band D has to be related to the ionizations from 16a″ and 24a′ MOs. The increase in relative intensity of the broad band B on passing to the more energetic radiation allows us to assign it to ionizations from five ruthenium-localized MOs (28a′, 27a′, 26a′, 18a″, 25a′). The shift toward higher IEs of band B with respect to the corresponding band of **I** can be ascribed with confidence to the smaller relaxation phenomena[26] associated with 4d-based MOs with respect to the 3d ones. Band B′ has to be related to the ionization from the 19a″ MO, namely a metallic 4d pair destabilized by an antibonding interaction with ligand-based orbitals. This assignment is substantiated by the decrease in relative intensity of this band under He II radiation,[23] in agreement with the high contribution of C_{2p} AOs to the 19a″ MO (Table IV). Theoretical results (Tables III and IV) suggest for this MO a stronger antibonding character in **II** than in **I**, probably due to a better energy matching between the interacting metal and ligand levels. Finally, band A is assigned with confidence to the ionization from the 29a′ HOMO.

$Os_2(CO)_6(C_4H_4)$. Because of the nonrelativistic nature of the theoretical scheme used, we must consider the results at a semiquantitative level; moreover, since the Mulliken population analysis[11] suffers well-known limitations when dealing with third-series transition metals,[27] we do not report for **III** a detailed charge density analysis of each MO but will only underline some interesting trends that can be drawn from the comparison with the results of **I** and **II** (Table I). In particular, it has been shown that the stronger M–M′ interaction in **II** with respect to that in **I** has significantly modified the nature of the interactions within the metallacycle. Moreover, the metal–metal interaction in **II** has been interpreted as a metal charge-balancing mechanism

(23) In fact, on the basis of the Gelius model,[24] we expect a marked decrease in the cross-section ratio σ(C 2p)/σ(M nd) on passing from the He I to the He II excitation source.

(24) Gelius, U. In *Electron Spectroscopy*; Shirley, D. A., Ed.; North-Holland: Amsterdam, 1972; p 311.
(25) Slater's transition-state calculations[9] have been performed for each single MO reported in Tables II–IV. Relative results are summarized in Figure 2.
(26) Calabro, D. C.; Lichtenberger, D. L. *Inorg. Chem.* **1980**, *19*, 1732.
(27) Noel, J. O. *Inorg. Chem.* **1982**, *21*, 11.

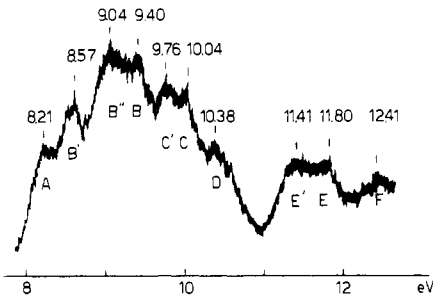

Figure 12. He I PE spectrum of $Os_2(CO)_6(C_4H_4)$.

competitive with the M → π_3*(C_4H_4) and M → π*(semibridging CO) back-donations. An even stronger metal–metal interaction is expected and actually computed for **III** (Table I). On this basis, one could tentatively explain the sawhorse geometry of **III**, because no semibridging carbonyl is now necessary to balance metal charges. The very strong metal–metal bond is consistent with the Os–Os′ bond length (2.75 Å),[5j] which is shorter than those observed in many cluster compounds,[28] including $Os_3(CO)_{12}$ itself (2.88 Å).[28d,e] It is of relevance to point out that almost all a′ type MOs participate in the metal–metal bond with a large contribution from the HOMO (see relative CP in Figure 11).

The experimental PE pattern of **III** below 12.5 eV (see Figure 12) is much more structured than those of **I** and **II**. The assignments are quite straightforward by reference to the discussion of **I** and **II** and to the TSIEs of Figure 2. In Figure 12 one can single out at least 10 well-resolved bands. Band A is once again assigned to the ionization from the HOMO 29a′, while band B′ is related to the ionization from the 19a″ MO. The existence of the resolved band B′ in **III** supports the theoretically expected antibonding interaction between the nd AO and ligand-based orbitals becoming stronger along the series Fe → Ru → Os. Bands B and C are both split into two components (B″, B and C′, C, respectively) with relative intensity 2:1:1:1. Believing in the TSIE ordering obtained by the present nonrelativistic calculations, one could tentatively assign band B″ to the ionization from the 28a′ and 18a″ MOs, while the three subsequent bands could be associated with the ionizations from the 27a′, 26a′, and 17a″ MOs, respectively. Band D should be assigned to the ionization from the 25a′ MO, and bands E′, E, and F are associated with single ionization events (24a′, 16a″, and 23a′ MOs, respectively).

Concluding Remarks

The present study has demonstrated that in polynuclear organometallic molecules the strength of the metal–metal bond can influence the nature of the metal–ligand interactions. Actually, in the present series of isoelectronic molecules, where only metals of the same group have been changed, significantly different bonding schemes have been found. Such differences have been traced back ultimately to differences in metal electronegativity and nd AO size. The role played by electronegativity is confirmed by structural data of a related heterobinuclear (Fe–Ru) cluster,[5h,29] where the metalla position is always occupied by the Ru atom, being less disposable than Fe in the formation of a dative metal–metal bond. Similar considerations have been previously invoked to explain the structure of $M_2M'(CO)_9(RC_2R)$ (M = Fe, M′ = Ru, R = C_6H_5; M = Fe, M′ = Ru, R = C_2H_5),[29] $H_2Os_3(CO)_9(RC_2R)$ (R = CH_3),[30] and $Fe_3(CO)_9(RC_2R)$ (R = CH_3)[31] complexes.

Acknowledgment. Financial support for this study from the Ministero della Pubblica Istruzione (Rome) is gratefully acknowledged. We thank F. De Zuane for technical assistance.

Registry No. $Fe_2(CO)_6(C_4H_4)$, 108034-90-8; $Ru_2(CO)_6(C_4H_4)$, 108034-91-9; $Os_2(CO)_6(C_4H_4)$, 108034-92-0.

(28) (a) Ferraris, G.; Gervasio, G. *J. Chem. Soc., Dalton Trans.* **1972**, 1057. (b) Bradford, C. W.; Nyholm, R. S.; Gainsford, G. J.; Guss, J. M.; Ireland, P. R.; Mason, R. *J. Chem. Soc., Chem. Commun.* **1972**, 87. (c) Deeming, A. J.; Underhill, M. *J. Chem. Soc., Chem. Commun.* **1973**, 277. (d) Corey, E. R.; Dahl, L. F. *Inorg. Chem.* **1962**, *1*, 521. (e) Churchill, M. R.; DeBoer, B. G. *Inorg. Chem.* **1977**, *16*, 878.

(29) Busetti, V.; Granozzi, G.; Aime, S.; Gobetto, R.; Osella, D. *Organometallics* **1984**, *3*, 1510.

(30) Bertoncello, R.; Granozzi, G.; Busetti, V.; Aime, S.; Gobetto, R.; Osella, D. *Inorg. Chem.* **1986**, *25*, 4004.

(31) Granozzi, G.; Tondello, E.; Casarin, M.; Aime, S.; Osella, D. *Organometallics* **1983**, *2*, 430.

Contribution from the Laboratoires de Chimie (UA CNRS 1194) et Service de Physique, Dêpartement de Recherche Fondamentale, CENG, 85X F 38041 Grenoble Cédex, France

Structural and Magnetic Properties of a Novel Pentacopper(II) Cluster Involving a Trinucleating Catechol Ligand

Eric Gojon,[1a] Jacques Gaillard,[1b] Jean-Marc Latour,*[1a] and Jean Laugier[1b]

Received October 15, 1986

The structure of $Cu_5(OH)_2(L)_2(NO_3)_4 \cdot 2.5H_2O$, where H_2L is the new ligand 3,6-bis((4-methylpiperazino)methyl)pyrocatechol, has been determined by X-ray diffraction techniques to a final discrepancy index of $R = 0.049$. The complex crystallizes in the space group $P2_1/n$ with four molecules per unit cell having the dimensions $a = 15.559$ (3) Å, $b = 13.417$ (3) Å, $c = 24.638$ (8) Å, and $\beta = 99.03$ (1) °. The five copper atoms are arranged as a rectangular based pyramid. The copper atoms at the short edges of the rectangle are bridged by a hydroxide while those at the long edges are bridged by the catecholate ligand. The apical copper is bridged to each of the other copper atoms by a catecholate oxygen. Magnetic susceptibility data over the range 5–300 K and EPR experiments near helium temperature have been used to investigate the magnetic interactions within the pentanuclear cluster. The hydroxide-bridged coppers experience exchange interactions of ca. −80 and −145 cm^{-1} while the apical copper is more weakly coupled to the four others. These results are discussed with the help of the magnetic orbital concept.

Introduction

Catechols are ubiquitous in biology where they can act as electron donors,[2] complexing agents in carrier proteins,[3] and substrates, intermediates, or products of oxidative reactions.[4] In most of these processes, the catechols are found to interact with transition-metal ions, iron and copper mainly. This has led, in the recent past, to a surge of interest in transition-metal catecholates.[5] Solution studies have demonstrated the high affinity of catecholates for the cupric ion, especially when nitrogen ligands are associated with catechols in the copper coordination sphere.[6] Most of the early work was aimed at studying the copper-catalyzed

(1) (a) Laboratoires de Chimie. (b) Service de Physique.

(2) Reinhammar, B. In *Copper Proteins and Copper Enzymes*; Lontie, R., Ed., CRC Press: Boca Raton, FL, 1984; Vol. III, Chapter 1, pp 1–35.

(3) Raymond, K. N.; Carrano, C. J. *Acc. Chem. Res.* **1979**, *12*, 183–190.

(4) (a) Lerch, K. *Met. Ions Biol. Syst.* **1981**, *13*, 143–186. (b) Que, L. *Struct. Bonding (Berlin)* **1980**, *40*, 39–72.

(5) Pierpont, C. G.; Buchanan, R. M. *Coord. Chem. Rev.* **1981**, *38*, 45–87.

(6) Sigel, H. *Inorg. Chem.* **1980**, *19*, 1411–1413.

0020-1669/87/1326-2046$01.50/0